Photonic and plasmonic surface field distributions characterized with normal- and oblique-incidence multi-photon PEEM

Robert C. Word*, Rolf Könenkamp

Portland State University, Department of Physics, P.O. Box 751, Portland, OR 97207, USA

ARTICLE INFO

ABSTRACT

Photonic and plasmonic fields at surfaces can have complicated spatial distributions, which are reflected in the corresponding photoelectron yields imaged in PEEM. These can include the intricate moiré patterns on the surfaces of photonic and plasmonic structures and bright fringe field patterns at their edges. Understanding field distributions requires an understanding of how the guided modes develop, propagate, and interfere with each other and with the incident far-field light. Recent efforts in PEEM include the use of normal incidence excitation in addition to or in lieu of oblique incidence to alter the yield distributions. In this paper we present three cases of surface near-fields imaged in PEEM: an indium tin oxide photonic waveguide, a large gold plasmonic patch antenna, and a small gold plasmonic slot antenna. We show that the surface fields of the waveguide are those of a dual-mode waveguide and that the fields of the plasmonic antennas arise from the asymmetric surface plasmon mode excited at the perimeter of the antennas. We analyze the photoelectron yield distributions and compare and contrast the use of normal and oblique incidence for each case.

© 2017 Elsevier B.V. All rights reserved.

1. Introduction

Multi-photon photoemission electron microscopy or nP-PEEM has seen extensive use for observation of plasmonic and photonic phenomena. Of particular interest are plasmonic antennas, which may fulfill elementary circuit functions such as light routing [1], switching [2], and coherent control processes [3] on the nanometer scale. There are, however, significant challenges inherent to surface plasmons such as the potential for high energy losses. Furthermore, the various surfaces of antenna, such as its perimeter, top, and bottom surfaces, can develop their own resonances and the combined field structure can be complicated. We have recently addressed the possibility of using nP-PEEM's high spatial resolution and contrast to characterize micrometer-sized optical waveguides and plasmonic antenna structures [4–7].

The underlying idea is that areas of high electromagnetic field intensities generate high photoelectron yields with a spatial distribution that to a first approximation is given by

$$Y(r) \propto \int |E|^{2n} dt, \qquad (1)$$

in which the net electric field E enhances the n-photon photoemission (nPPE) yield by a factor of $2n$, with n being the number of photons needed to overcome the work function of the material. An unknown factor in this equation is the probability of a photoemission event, but generally, the higher n, the lower the probability, and by a significant margin [8]. To overcome poor emission rates for $n > 1$, practical nP-PEEM requires ultrafast lasers with pulse widths less than ~100 fs, pulse rates in the order of ~100 MHz, and high average powers (100 mW to 1 W).

Due to limitations inherent to combining electron optical elements with light optics, PEEM usually employs a fixed oblique angle of incidence of $\theta = 60°$ or greater. This introduces complications to the interpretation of field distributions by introducing an in-plane directional component to the excitation light. More specific to the study of plasmonic antennas, oblique incidence may also limit the types of resonant modes that can be excited. Broadly speaking, dipole antenna resonance is the most technologically useful, and in most cases normal incidence is the optimal way to achieve it. On the other hand, oblique incidence reduces symmetry and allows for the excitation of multipolar modes [7,9,10].

To employ normal incidence in PEEM one has to overcome the design limitations imposed by the electron optics. One method is to direct the laser through the apertures of the electron objective lens. This is achieved in SPECS-type instruments by inserting a small mirror close to the electron optical path [9]. Another approach avoids disturbance to the electron optics by taking advantage of an entry point much further away, at the junction of the "Y" of the Elmitec PEEM's beam line [11,12]. Another method is to install a mirror inside the sample stage [13] and direct the beam through the sample, achieving normal incidence via optical trans-

* Corresponding author.
E-mail address: wordr@pdx.edu (R.C. Word).
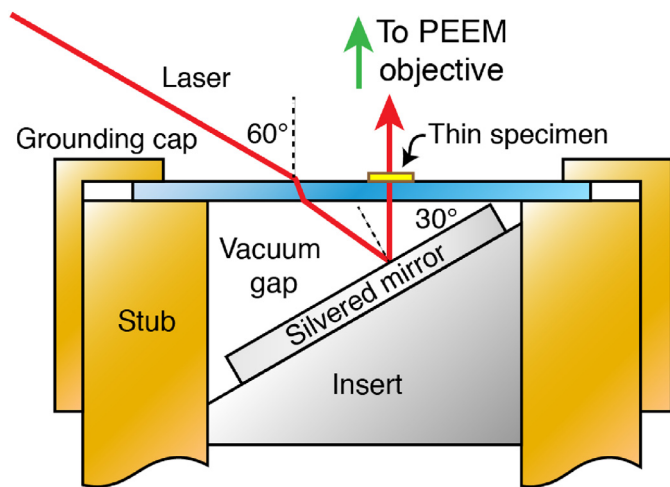
Fig. 1. Cut-away of a PEEM specimen stub. A transparent substrate, such as ITO-coated glass, allows the use of a small mirror to achieve normal incidence in PEEM. The diameter of the sample stub is 6.35 mm.
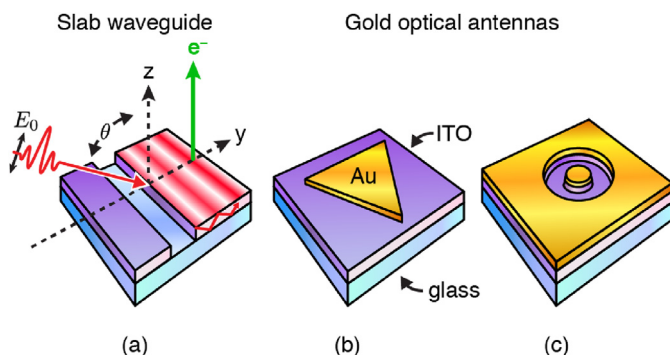
Fig. 2. Experimental schemes: (a) a slab waveguide in which light enters an ITO film via diffraction at a slot, (b) a single crystalline gold antenna, and (c) a slot antenna milled from a gold film. In each case, a femto-second pulse laser is incident at oblique ($\theta = 60°$) or normal incidence. Photoelectrons are accelerated away from the surface and imaged in an electron microscope.

mission. The specimen must be either very thin or transparent, such as an indium tin oxide substrate. In our approach we employ a small mirror within the specimen holder to achieve normal incidence from the bottom of the sample as shown in Fig. 1. The oblique-incidence laser beam is aligned such that it passes through the transparent substrate to the mirror where and it is reflected back again towards the specimen but at normal incidence. By installing the mirror inside the specimen holder 0° and 60° incidence may be selected for by only a small realignment of the laser.

The aim of this report is to compare and contrast the two types of far-field excitation typically used in PEEM in terms of three types of photonic and plasmonic structures: a simple thin film multi-mode waveguide, a large plasmonic antenna structure, and a sub-micron plasmonic antenna structure as shown in Fig. 2. In each case we present nP-PEEM images taken using both oblique and normal incidence. We discuss analytical models for interpreting the yield distributions seen in the images and remark on advantages or disadvantages that may arise from use of the individual angles.

2. Experimental details

Common to all three specimens shown in Fig. 2 is a substrate of ITO-coated glass coverslips (SPI, Supplies), which have an ITO thickness of 250 nm and a measured sheet resistance of about 15

$\Omega/\square$. The simple slab waveguide (Fig. 2(a)) was made by milling a long groove, 1-μm across and 200-nm deep, into the ITO with an FEI Strata dual-beam FIB. The plasmonic antennas were made from single-crystalline gold platelets produced via the auric acid reduction method of Guo et al. [14]. The resulting hexagonal and triangular gold platelets have lateral dimensions on the scale of microns and thicknesses in the range of 50 to 100 nm. These were drop-deposited on ITO substrates and imaged as-deposited (Fig. 2(b)) or used as a basis to prepare annular slot antennas with the FIB. In the latter case we applied the circular raster function of the FIB set to the lowest possible beam current (1 pA) for ~30 seconds per antenna.

Images were taken with our home-built aberration-corrected PEEM, which employs a Spectra-Physics MaiTai Ti: sapphire laser with an average output power of 1-watt, a pulse width of 60 fs, and repetition rate 80 MHz. The laser wavelength used was $\lambda_L = 800$ nm or 400 nm, the latter obtained with a Del Mar harmonic generator. Polarization was set with a tunable wave plate. The spot size of the laser on the specimen was ~100 μm. Image exposure times were about 1 minute and were recorded by a CCD camera, which was optically coupled to a phosphor screen.

3. Results and discussion

3.1. Photonic waveguide

We begin with the photonic case of a simple slab waveguide imaged with $\lambda_L = 400$ nm TM light as shown in Fig. 2(a). In this case, light from the laser scatters off of a groove milled into the ITO thin film, which is arranged roughly perpendicular to the plane of incidence. Via diffraction, some of the scattered light enters the film and propagates as one or more guided modes. The thickness of the film (250 nm) and its index of refraction ($n_2 = 2.1$; ref. [15]) as well as the indices of adjacent layers (vacuum $n_1 = 1$, and BK7 glass, $n_3 = 1.51$) impose selection rules on the guided modes that can propagate within the film [16]. In the 2P-PEEM images shown in Fig. 3(a) and 3(b), we see a series of bright and dark bands, which are the result of interference between the incident light and the guided light. In the first case, the laser was incident at 60° The interference pattern is skewed downward in direction of the incident light and is strongest when the guided and incident light share a common direction. In Fig. 3(b) the laser was incidence at 0° and the resulting interference pattern surrounds the central groove with equally spaced fringes. As an indication that the transmitted angle of incidence is indeed close to 0°, we see nearly circular fringes around particles outside the groove. In each case, we can analyze the interference pattern and determine the velocity or effective index of the guided modes. Here we outline the case for a single-mode waveguide, but the principal is the same for the multi-mode waveguide used in the experiment.

The fringe spacing or fringe wavelength λ_m of the interference pattern is defined by the fringe's wave vector $\vec{k}_m$, which is always perpendicular to the fringes,

$$\lambda_m = \frac{2\pi}{\left|\vec{k}_m\right|}. \qquad (2)$$

As explained by Kahl and coworkers [17], the wave vector of the fringe pattern in three-dimensional space is the difference,

$$\vec{k}_m = \vec{k}_S - \vec{k}_L, \qquad (3)$$

in which $\vec{k}_L$ is the wave vector of the incident light and $\vec{k}_L$ is the wave vector of the guided light. Since PEEM is concerned with the surface of the slab waveguide, we can reduce the problem to two dimensions as

$$\vec{k}_m = \vec{k}_{eff} - \vec{k}_L^{\parallel}, \qquad (4)$$